

Dissipative Currents in Superfluid ^3He Weak Links

J. K. Viljas¹ and E. V. Thuneberg^{1,2}

¹*Low Temperature Laboratory, Helsinki University of Technology, P.O.Box 2200, FIN-02015 HUT, Finland*

²*Department of Physical Sciences, P.O.Box 3000, FIN-90014 University of Oulu, Finland*

(Dated: November 21, 2018)

We calculate the current-pressure relation for pinholes connecting two volumes of bulk superfluid ^3He -B. The theory of multiple Andreev reflections, adapted from superconducting weak links, leads to a nonlinear dependence of the dc current on pressure bias. In arrays of pinholes one has to take into account oscillations of the texture at the Josephson frequency. The associated radiation of spin waves from the junction leads to an additional dissipative current at small biases, in agreement with measurements.

PACS numbers: 67.57.De, 67.57.Fg, 67.57.Np

Weak links between superconducting metals have been extensively studied during the past 40 years. More recently, similar experiments have also been made in atomic superfluids, in the fermion ^3He liquid in particular [1]. Experiments in superfluids can shed new light on general weak link phenomena, due to the availability of parameter ranges which are not easily realized in superconductors. There is also intrinsic interest in superfluids since completely new phenomena may appear which are not possible in conventional superconductors. Previous work on ^3He weak links has mostly concentrated on determining the equilibrium properties, like the Josephson current-phase relation $I(\phi)$. A new phenomenon identified in this context is the *anisotextural* effect, where spin-orbit degrees of freedom change as a function of the phase difference ϕ . As a consequence $I(\phi)$ deviates essentially from the sinusoidal form $I = I_c \sin \phi$ so that there appear π states, where both derivatives $I'(0)$ and $I'(\pi)$ are positive [2, 3].

In this letter we present a theory of dissipative currents in superfluid ^3He weak links. Experimental studies of such time-averaged, or dc currents under a pressure bias have been reported in Refs. 4 and 5. At constant chemical potential difference U the supercurrent $I(\phi)$ oscillates at the Josephson frequency $\omega_J = 2U/\hbar$. Therefore the superfluid part does not contribute to the dc current unless there is a mechanism for absorbing the extra energy $2U$ per transported Cooper pair. One example is the process of multiple Andreev reflections (MAR), used for explaining properties of superconducting weak links [6, 7]. Due to Andreev reflection there are quasiparticle states bound to the contact region. These states carry the current, one Cooper pair per one back-and-forth reflection. Simultaneously the quasiparticles gain energy until they escape above the gap or are relaxed by scattering. This process works also in superfluid ^3He , but with important differences in details. Below we argue that in ^3He there is an additional dissipation mechanism. Owing to the anisotextural effect, energy can be carried away from the junction by spin-wave radiation. We show that the two mechanisms together can explain the essential features of the experimental results in Refs. 4 and 5.

Multiple Andreev reflections.—Let us consider a weak

link under constant difference U in chemical potentials. In ^3He U is related to the pressure difference P by $U = (m_3/\rho)P$, where ρ is the density and m_3 the mass of an atom. The time derivative of the phase difference ϕ across the link is given by the Josephson frequency $\dot{\phi} = \omega_J = 2U/\hbar$. The time-dependent mass current can then be expressed as a Fourier series

$$I(P, t) = I_0(P) + \sum_{n=1}^{\infty} [I_n^S(P) \sin(n\omega_J t) + I_n^C(P) \cos(n\omega_J t)] \quad (1)$$

with coefficients I_0, I_n^S, I_n^C . We have calculated these coefficients for a pinhole, where the dimensions of the hole are assumed small in comparison with the superfluid coherence length $\xi_0 = 77$ nm. (All parameters are evaluated at vapor pressure.) Our calculation uses nonequilibrium Green's functions, and is explained in the appendix. However, a large part of the results can be understood by the following adiabatic model, which is a generalization of the one used for superconductors [7].

The current arises from quasiparticle states that are bound in the weak link at energies below the gap Δ . The mass current is given by

$$I(t) = \frac{m_3}{\hbar} \sum_i \sum_{\delta} \sum_n \sum_{\sigma} \frac{d\epsilon_{i\delta n\sigma}}{d\phi} p_{i\delta n\sigma}. \quad (2)$$

Here $\epsilon_{i\delta n\sigma}(\phi)$ is the bound state energy that depends on the channel index i , momentum sign $\delta = \pm$, and spin index $\sigma = \pm$. The index n is for the case that there exist more than one bound state. The distribution function $p_{i\delta n\sigma}(t, \phi)$ obeys the kinetic equation

$$\frac{\partial p_{i\delta n\sigma}}{\partial t} + \dot{\phi} \frac{\partial p_{i\delta n\sigma}}{\partial \phi} = \Gamma [f(\epsilon_{i\delta n\sigma}) - p_{i\delta n\sigma}], \quad (3)$$

where $f(\epsilon) = [\exp(\epsilon/k_B T) + 1]^{-1}$ is the Fermi distribution and Γ^{-1} a relaxation time.

Application of the above to ^3He includes a few specific features. First, the order parameter is always suppressed near walls. We calculate it self-consistently, assuming diffusive scattering of quasiparticles at the wall. This implies that also the energies $\epsilon_{i\delta n\sigma}(\phi)$ have to be calculated

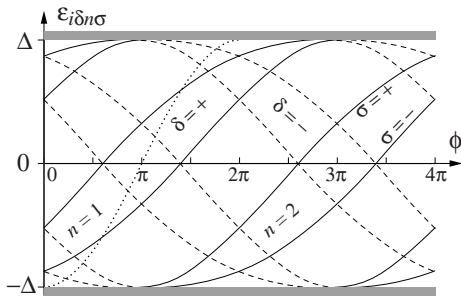


FIG. 1: The bound state energies $\epsilon_{i\delta n\sigma}$ as a function of the phase difference ϕ . Neglecting gap suppression $\epsilon_\delta = -\delta\Delta \cos(\phi/2)$ (dotted line). Parameters are: quasiparticle direction cosine 0.93, temperature $0.6T_c$ and $\mathbf{R}^{1,r} = \mathbf{R}(\mp\hat{z}, \theta_L)$.

numerically. One example is shown in Fig. 1. Second, since we consider the B phase, the bulk order parameter is of the form $\Delta \mathbf{R} \exp(i\phi)$, where \mathbf{R} is a rotation matrix [8]. Depending on the matrices on the left (l) and right (r) hand sides, $\mathbf{R}^{1,r}$, there is spin-splitting: $\epsilon_{i\delta n-}(\phi) \approx \epsilon_{i\delta n+}(\phi - \psi)$ [9, 10]. Third, the only important source of inelastic processes is quasiparticle-quasiparticle collisions. Near a surface the order parameter is suppressed and therefore we approximate the scattering rate by the normal Fermi-liquid form $\Gamma = a[(\pi k_B T)^2 + \epsilon^2]/(\tau_0 \pi^2 k_B^2)$. Here $\tau_0 = 1.14 \mu\text{s mK}^2$ is obtained from viscosity measurements and a is a coefficient on the order of unity. The low-energy Γ is denoted by $\Gamma_0 = aT^2/\tau_0$.

We are now equipped to analyze Fig. 2. Similar to the experiments, we study the low-bias region, $U \ll k_B T_c$. In this region we can neglect the normal current from energies above Δ , excluding only a narrow temperature slice near the superfluid transition temperature T_c . A characteristic scale for U is set by the scattering strength $\hbar\Gamma$. At $U = 0$, the distribution function is in equilibrium, $p_{i\delta n\sigma} = f(\epsilon_{i\delta n\sigma})$. Equation (2) then gives the equilibrium current-phase relation $I(\phi)$, dominated by $\sin(\phi)$ (at least for $\mathbf{R}^l = \mathbf{R}^r$) but with smaller admixtures of $\sin(n\phi)$ where $n > 1$. At $U \ll \hbar\Gamma$ the kinetic equation (3) can easily be solved by linearization. This leads to a time-independent component I_0 that is linear in U and independent of $\mathbf{R}^{1,r}$,

$$I_0 = g(T)(\Delta/\hbar\Gamma_0)G_n U. \quad (4)$$

Here G_n is the normal-state conductance and $g(T)$ a factor on the order of unity. Neglecting gap suppression, $g(T) = \int_{-1}^1 \tanh(\Delta x/2k_B T)(x/\sqrt{1-x^2})dx$. The validity region of the linear dependence (4) vanishes as $T \rightarrow 0$ and is replaced by $I_0 \propto U^{1/3}$. Finally, at $U \gg \hbar\Gamma$ (but still $U \ll \Delta$) the scattering can be neglected and p is determined by thermalization at gap edges, $p_{i\delta n\sigma} = f(-\delta\Delta)$. Here I_0 approaches a constant value that is on the same order as the critical current. For a self-consistent order parameter all higher harmonics are effectively damped by the smooth $\epsilon_{i\delta n\sigma}(\phi)$.

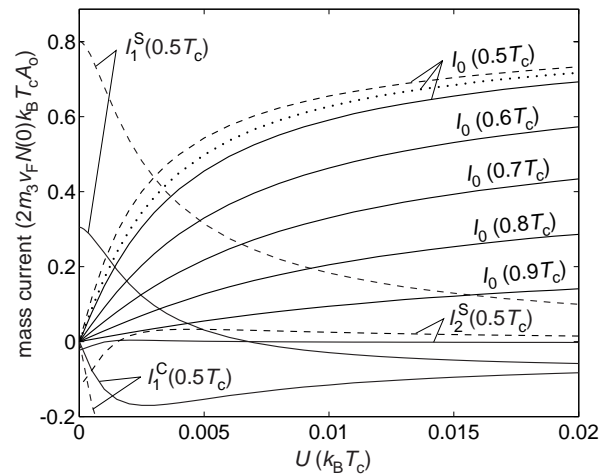


FIG. 2: Current amplitudes I_0 , I_1^S , I_2^S and I_1^C (1) as functions of the chemical potential difference U . The average current I_0 is shown at different temperatures, other curves are for $T/T_c = 0.5$. I_0 is linear at small U (4) and saturates at larger U , as discussed in the main text. The most accurate results are shown by solid lines. The effect of neglecting the gap suppression is shown by dashed lines, and the effect of neglecting the energy dependence of Γ is shown by a dotted line. The largest shown bias is $P \approx 4.2$ Pa. Parameters are $a = 1.6$ and $\mathbf{R}^l = \mathbf{R}^r$.

The $I_0(P)$ in Fig. 2 can be compared with the measurements in Ref. 4. They have the same shape and a good order-of-magnitude agreement on both axes. The agreement is surprisingly good taking into account that the aperture sizes are on the order of ξ_0 or larger, and thus our pinhole approximation is not justified.

The more recent experiment of Ref. 5 was done with an array of apertures. In contrast to Ref. 4, this experiment should be well in the region where the linear approximation (4) is valid. However, a clearly nonlinear $I-P$ curve was measured. The experimental results are also different for the two possible states of the weak link, the “H” and the “L” states, which have previously been identified as two nearly degenerate textural states with different $\mathbf{R}^{1,r}$'s [3]. Yet, our numerical calculations confirm that $I_0(P)$ curves in Fig. 2 remain practically unchanged for all $\mathbf{R}^{1,r}$. This can also be seen in the adiabatic model as follows. The spin splitting $\epsilon_{i\delta n-}(\phi) \approx \epsilon_{i\delta n+}(\phi - \psi)$ has an essential effect on the critical current so that I_1^S can even vanish [10]. In I_0 , however, the relative phase shift is unimportant since the phase runs through all values.

We conclude that the nonlinearity and the texture-dependence in Ref. 5 are either large-aperture effects, and/or result from something other than MAR. In the following we demonstrate that at least part of the H-L difference can be accounted for by the anisotextural effect, which exists in array-type weak links of $^3\text{He-B}$.

The anisotextural model.—As discussed above, the current-phase relation $I(\phi)$ depends on the rotation ma-

trices $R^{l,r}$. The basic idea of the anisotextural effect is that $R^{l,r}$ are not fixed, but tend to move toward their ϕ -dependent equilibrium configuration. This effect was previously used to explain the so-called π states, where a local minimum of energy appears at $\phi \approx \pi$ [3]. Below we generalize this theory to the dynamical case where $\phi(t) = \omega_J t$.

A simple but still realistic model for the anisotextural effect in an array of apertures is based on the energy functional [3]

$$F[\eta] = F_J(\eta_0, \phi) + \frac{1}{2}K \int d^3r |\nabla\eta|^2. \quad (5)$$

Here F_J is the Josephson coupling energy and the second term is due to the bending of the rotation axis $\hat{\mathbf{n}}$ which parametrizes the matrix $R(\hat{\mathbf{n}}, \theta_L)$. The rotation angle is fixed to $\theta_L \approx 104^\circ$ by the bulk dipole-dipole interaction [11]. Due to the geometry of the experiment [5], we assume $\hat{\mathbf{n}}$ to be fixed parallel to the wall normal $\hat{\mathbf{z}}$ on one side of the array. On the other side $\hat{\mathbf{n}}$ makes an angle $\eta(r)$ with $\hat{\mathbf{z}}$, which depends on the distance r from the center of the array. We choose a cutoff at $r = r_0$, below which $\eta(r)$ is assumed constant (see inset in Fig. 3). The F_J term depends on the angle $\eta_0 \equiv \eta(r_0)$ near the junction, and the bending term is nonzero if η_0 differs from $\eta_\infty \equiv \eta(\infty)$ preferred by walls and other textural interactions. At temperatures near T_c the energy F_J can be approximated by $F_J = -E_J \cos \phi$ where $E_J = \alpha R_{\mu z}^l R_{\mu z}^r + \beta (R_{\mu x}^l R_{\mu x}^r + R_{\mu y}^l R_{\mu y}^r)$. We choose to fix the r side ($\hat{\mathbf{n}}^r \parallel \hat{\mathbf{z}}$), and on the l side it is convenient to take $0 < \eta_\infty < \pi/2$. The H and L states are then identified as the states with $\hat{\mathbf{n}}^r = \pm \hat{\mathbf{z}}$, respectively [3]. Linearizing around $\eta \approx \eta_\infty$, we find $E_J \approx E_J^\infty - J_{\text{sp}}\vartheta(r_0)$, where $\vartheta = \eta - \eta_\infty$, and $J_{\text{sp}}(\eta_\infty) = [\pm(20\alpha + 5\beta) \sin 2\eta_\infty + 30\beta \sin \eta_\infty]/16$. The coefficients α , β and K are calculated in Ref. 3.

The dynamics is determined by the Leggett equations $\dot{S} = -\delta F/\delta\theta$ and $\dot{\theta} = \mu_0\gamma_g^2 S/\chi$ [11]. Here the spin S and spin-rotation angle $\theta = \sqrt{5/2}\vartheta$ are conjugate variables. γ_g is the gyromagnetic ratio and χ the spin susceptibility. [The Leggett equations are canonical equations for a Hamiltonian where the spin energy density $\mu_0\gamma_g^2 S^2/2\chi$ is added to F in Eq. (5)]. The dynamical equations reduce to a wave equation in the bulk and F_J determines a boundary condition at the junction. The solution at constant P consists of waves that propagate radially out of the junction. This implies that the supercurrent $I_s = (2m_3/\hbar)\partial_\phi F_J(\eta_0, \phi)$ has a nonzero average, the anisotextural current

$$I_{\text{ai}}(P) = \frac{2m_3}{\hbar} \frac{[J_{\text{sp}}(\eta_\infty)]^2}{4\gamma} \frac{\omega_J r_0/c}{1 + (\omega_J r_0/c)^2}. \quad (6)$$

Here $c = \sqrt{2\mu_0\gamma_g^2 K/(5\chi)}$ is the spin-wave velocity and $\gamma = b\pi K r_0$. We estimate $r_0 = \sqrt{A/\pi}$, where A is the surface area of the array. We also take into account that the actual geometry around the junction differs from a half-space and use $b = 0.31$ instead of unity [3].

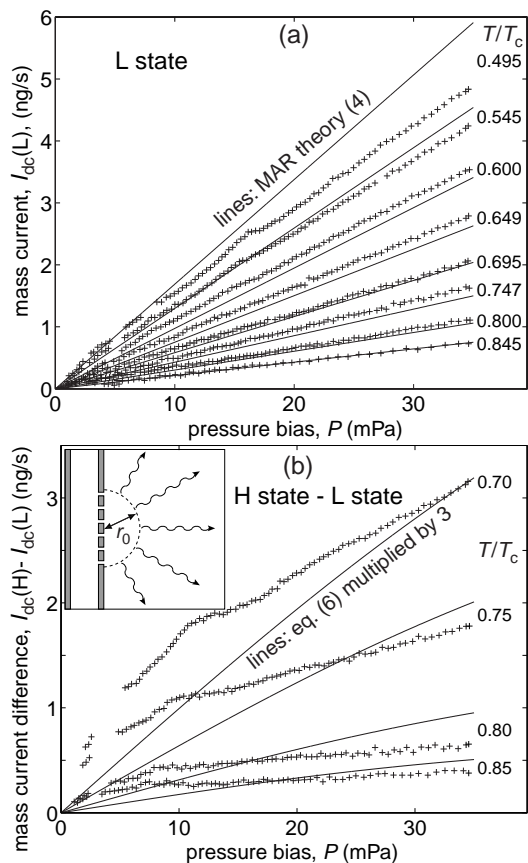


FIG. 3: Comparison of experimental [5] (+) and theoretical (solid lines) current-pressure relations. (a) The L state current is compared with theoretical I_0 (4) with a single adjustable parameter $a = 1.6$ coming from the collision rate Γ . (Alternatively, one can neglect the gap suppression and use $a = 3.2$.) (b) The difference between the H and L state currents is compared with the difference of I_{ai} (6), which is arbitrarily multiplied by factor 3. The inset depicts the Josephson array, cut-off radius r_0 , and radiation of spin waves.

The crucial features of the anisotextural current I_{ai} (6) are the dependence on the textural configuration via $J_{\text{sp}}(\eta_\infty)$, and the nonlinear dependence on pressure via ω_J . The origin of I_{ai} is the oscillating part in Eq. (1), which was here approximated by the I_1^S term alone. The total dc current I_{dc} is the sum of I_{ai} and the constant component due to MAR, $I_{\text{dc}} = I_0 + I_{\text{ai}}$.

Comparison to experiments.— It turns out that the L state current, which is rather linear [5], can almost completely be attributed to MAR. The comparison of the L state data with I_0 is presented in Fig. 3(a). There is only one adjustable parameter $a \sim 1$, which is associated with the uncertainty of the relaxation rate Γ . A likely reason for the differences is that the theory uses the pinhole approximation, which is not strictly valid for the experimental apertures (100 nm \times 100 nm squares in a wall of thickness 50 nm are not small compared to $\xi_0 = 77$ nm).

Since both the H and L state data are assumed to con-

tain the same contribution I_0 , it is convenient to subtract the H and L state data taken at equal temperatures. In this way one may directly compare the texture-dependent parts with I_{ai} , regardless of any uncertainty that may be present in I_0 . This is done in Fig. 3(b). The theoretical result corresponds to the difference between Eq. (6) calculated for the two states. There are no adjustable parameters, since the only free parameter is the textural angle η_∞ , which was previously found to be approximately 0.3π based on static properties [3]. The anisotextural model, as presented above, can explain roughly one third of the observed H-L difference. [The theoretical current in Fig. 3(b) is arbitrarily multiplied by factor 3 in order to make it better visible.] Also, the curvature in the theoretical lines is at higher biases than in the experimental results. There are several possible sources for the differences, in particular the oversimplifications used in our anisotextural model. Unfortunately, it would be very demanding to improve upon the pinhole approximation, or to calculate the texture and propagation of spin waves in the complicated geometry of the experiment [3]. There is also uncertainty in the experimental parameters, for example in the diameter of the apertures, which appears in its fourth power in I_{ai} . As a result, the true reason for the factor-of-three discrepancy remains open.

Conclusion.—We have presented a theory of dissipative currents in ^3He weak links. It shows that the nonlinearities in the measurements of Refs. 4 and 5 have different origins, and both can semi-quantitatively be explained by natural extensions of existing theories. The extension of static anisotextural phenomena to dynamics gives further support for the theory, and provides the energy loss mechanism that is required for a weak link to become trapped in a π state, as seen in experiments [1]. The anisotextural phenomena are sensitive to the experimental cell and magnetic field, for example, and thus can be tested in detail in future experiments. Also the oscillating components I_n^S and I_n^C in Fig. 1 as well as the spin waves might be observable in experiments.

Appendix: Calculation of currents.—Consider a pinhole with open area A_o . Assume the l-side chemical potential to be shifted by U with respect to the r side, and take the z axis to point from l to r. We define

G_n in Eq. (4) as $G_n = \frac{1}{2}m_3v_F N(0)A_o$, where $N(0)$ is the single-spin density of states in the normal state and v_F the Fermi velocity [3]. The mass current may then be written as $I(t) = G_n \langle \hat{k}_z I(\hat{\mathbf{k}}, t) \rangle_{\hat{k}_z > 0}$ where $\langle \dots \rangle_{\hat{k}_z > 0} = \int_{\hat{k}_z > 0} (d\Omega_{\hat{\mathbf{k}}}/4\pi) \dots$ denotes an average over the Fermi-surface points $\hat{\mathbf{k}}$. Since $I(t)$ is periodic with period $T_J = 2\pi/\omega_J$, we expand $I(\hat{\mathbf{k}}, t) = \sum_{n=-\infty}^{\infty} I_n(\hat{\mathbf{k}}) e^{in\omega_J t}$ such that $I_n(\hat{\mathbf{k}}) = I_{-n}^*(\hat{\mathbf{k}})$. Using the $\underline{\gamma}$ matrices of Ref. 12 to expand the Keldysh function, the amplitudes for $n \geq 0$ may be written as $I_n(\hat{\mathbf{k}}) = \text{Tr} \underline{C} \{ 2U\delta_{n0} - \sum_{m=0}^{\infty} \mathcal{P} \int d\epsilon [\underline{F}_{lr}^{m, m+n}(\hat{\mathbf{k}}, \epsilon, U) - \underline{F}_{rl}^{m+n, m}(-\hat{\mathbf{k}}, \epsilon, -U)] \}$ where $\underline{F}_{ij}^{l, m}(\hat{\mathbf{k}}, \epsilon, U) = \underline{P}_{ij}^m(\epsilon, U) [\underline{x}^i(\epsilon) - \underline{\gamma}^{Ri}(\epsilon) \underline{\tilde{x}}^j(\epsilon - U) \underline{\tilde{\gamma}}^{Ai}(\epsilon)] [\underline{P}_{ij}^l(\epsilon, U)]^\dagger$ and $\underline{P}_{ij}^m(\epsilon, U) = \prod_{p=0}^{m-1} \underline{\gamma}^{Ri}(\epsilon + (2p+2)U) \underline{\tilde{\gamma}}^{Rj}(\epsilon + (2p+1)U)$ where $i, j = l, r$, $\underline{C} = \underline{1}$, and $\hat{\mathbf{k}}$ dependences are omitted for clarity. (For spin current, replace $m_3 \rightarrow \hbar/2$ and $\underline{C} \rightarrow \underline{\sigma}$.) Since we are considering a pinhole, the l and r order parameters may be assumed to be unaffected by the weak link and to be in equilibrium. Thus the distribution functions are of the form $\underline{x}^i(\epsilon) = h^i(\epsilon) [\underline{1} - \underline{\gamma}^{Ri}(\epsilon) \underline{\tilde{\gamma}}^{Ai}(\epsilon)]$ and $h^i(\epsilon) = 1 - 2f(\epsilon)$. The conjugation symbol “ \sim ” is defined as in Ref. [12] and the amplitudes satisfy $\underline{\tilde{\gamma}}^A = [\underline{\gamma}^R]^\dagger$.

Above the $\underline{\gamma}^{R, A}$'s refer to the coherence functions inside the junction. They are obtained by integrating the Riccati equation $i\hbar \mathbf{v}_F \cdot \nabla \underline{\gamma}_0^R = -2\epsilon^R \underline{\gamma}_0^R - \underline{\gamma}_0^R \underline{\Delta}_0 \underline{\gamma}_0^R - \underline{\Delta}_0$ on several trajectories toward the wall on both sides, where $\epsilon^R = \epsilon + i(\hbar\Gamma/2)$, $\underline{\Delta}_0 = \underline{\Delta}_0 \cdot \underline{\sigma}_i \underline{\sigma}_2$, $\underline{\Delta}_0(\hat{\mathbf{k}}, z) = (\Delta_{\parallel} \hat{k}_x, \Delta_{\parallel} \hat{k}_y, \Delta_{\perp} \hat{k}_z)$, and $\Delta_{\parallel}(z)$, $\Delta_{\perp}(z)$ are calculated with the “ROM” model of a diffusive surface (cf. Ref. [3]). For a symmetrical junction, the l and r solutions at the junction satisfy $\underline{\gamma}_0^{Rr}(-\hat{\mathbf{k}}) = -[\underline{\gamma}_0^{Rl}(\hat{\mathbf{k}})]^T$. The different spin rotations $\underline{U}^{l, r} = \exp(-i\theta_L \hat{\mathbf{n}}^{l, r} \cdot \underline{\sigma}/2)$ are taken into account by writing $\underline{\gamma}^{Ri} = \underline{U}^i \underline{\gamma}_0^{Ri} [\underline{U}^i]^T$, for $i = l, r$.

The current amplitudes of Eq. (1) in Fig. 2 are obtained with $I_0 = G_n \langle \hat{k}_z I_0(\hat{\mathbf{k}}) \rangle_{\hat{k}_z > 0}$, $I_n^S = 2G_n \text{Im} \langle \hat{k}_z I_n(\hat{\mathbf{k}}) \rangle_{\hat{k}_z > 0}$, $I_n^C = 2G_n \text{Re} \langle \hat{k}_z I_n(\hat{\mathbf{k}}) \rangle_{\hat{k}_z > 0}$. These results have been derived for time-independent $\mathbf{R}^{l, r}$, but at least for $U \ll \hbar\Gamma_0$ we may expect them to be valid even if the textures vary on time scale T_J .

-
- [1] J.C. Davis and R.E. Packard, Rev. Mod. Phys. **74**, 741 (2002).
 - [2] J. K. Viljas and E. V. Thuneberg, Phys. Rev. Lett. **83**, 3868 (1999).
 - [3] J. K. Viljas and E. V. Thuneberg, Phys. Rev. B **65**, 064530 (2002).
 - [4] J. Steinhauer, *et al.*, Physica B **194-196**, 767 (1994).
 - [5] R. W. Simmonds, *et al.*, Phys. Rev. Lett. **84**, 6062 (2000).
 - [6] U. Gunsenheimer and A. D. Zaikin, Phys. Rev. B **50**, 6317 (1994).
 - [7] D. Averin and A. Bardas, Phys. Rev. Lett. **75**, 1831 (1995); Phys. Rev. B **53**, R1705 (1996).
 - [8] D. Vollhardt and P. Wölfle, *The superfluid phases of helium three* (Taylor & Francis, London, 1990).
 - [9] J. K. Viljas and E. V. Thuneberg, J. Low Temp. Phys. **134**, 743 (2004).
 - [10] S.-K. Yip, Phys. Rev. Lett **83**, 3864 (1999).
 - [11] A.J. Leggett, Ann. Phys. (New York) **85**, 11 (1974).
 - [12] M. Eschrig, Phys. Rev. B **61**, 9061 (2000).